IEEE Access
Multidisciplinary ⋮ Rapid Review ⋮ Open Access Journal

Received 29 June 2023, accepted 17 July 2023, date of publication 24 July 2023, date of current version 1 August 2023.

Digital Object Identifier 10.1109/ACCESS.2023.3298368

RESEARCH ARTICLE

Application of Reverberation Chamber for Radiated Emission Testing for Wireless Protection Toward Full-Scale Deployment of 5G System–Advantages and Challenges

IFONG WU, SADAAKI SHIOTA, YASUSHI MATSUMOTO, (Member, IEEE), AND KAORU GOTOH, (Member, IEEE)

National Institute of Information and Communications Technology, Koganei, Tokyo 184-8795, Japan

Corresponding author: Ifong Wu (ifong@nict.go.jp)

This work was partially supported by the Japan Society for the Promotion of Science (JSPS) KAKENHI Grant Number JP23K03808.

ABSTRACT With the widespread deployment of high-frequency wireless communication systems such as the fifth generation (5G) system, high-frequency electromagnetic (EM) disturbances have become prevalent, requiring high-frequency compatibility testing of radiated emissions to prevent unintentional EM disturbance. Generally, radiated emission testing is typically performed in a fully anechoic room (FAR). However, the reproducibility of test results has become a problem owing to the increased insertion losses in the measurement system and the complicated directivity of the radiation from the equipment under test as the frequency increases. As an alternative to the FAR, a reverberation chamber (RC) has attracted attention in recent years as it allows high-sensitivity measurement with compact equipment. To perform radiated emission testing in the RC, it is important that the detection value given by the specified detectors is not affected by the characteristics of the RC. However, the disturbance waveform received in the RC is generally different from that in the FAR, resulting in a different detector response. In this study, the detectors and resolution bandwidths (RBWs) for radiated emission testing were used to investigate the conditions under which the detection values measured in the RC were equivalent to those measured in the FAR. For root mean square detection, the dependence of the mean detection values measured in the RC on the pulse width and RBW agreed well with those measured in the FAR. However, the relative changes in the mean detection values of the peak and average detectors in the RC were different from those in the FAR unless the time constant of the RC multiplied by RBW was sufficiently smaller.

INDEX TERMS Average detector, electromagnetic disturbance, fully anechoic room, peak detector, radiated emission testing, reverberation chamber, root mean square detector.

I. INTRODUCTION

With the rapid spread of wireless communication systems and services such as the fifth-generation (5G) system, the frequencies used for these data communications have been increasing rapidly, reaching 28 GHz in Japan (see Fig. 1) [1], [2], [3], [4], [5], [6], [7], [8], [9]. This proliferation of frequencies has led to emerging electromagnetic compatibility (EMC) issues and the introduction of regulations and guidelines to address them [10], [11], [12]. Additionally, the electronic devices used for these systems and services have higher clock frequencies and data rates, which may create electromagnetic (EM) disturbances that could potentially interfere with other wireless communication systems and services [9]. To protect wireless communication systems from such unintended EM disturbance, radiated emission testing must be compatible with high frequencies.

The associate editor coordinating the review of this manuscript and approving it for publication was Jon Atli Benediktsson.

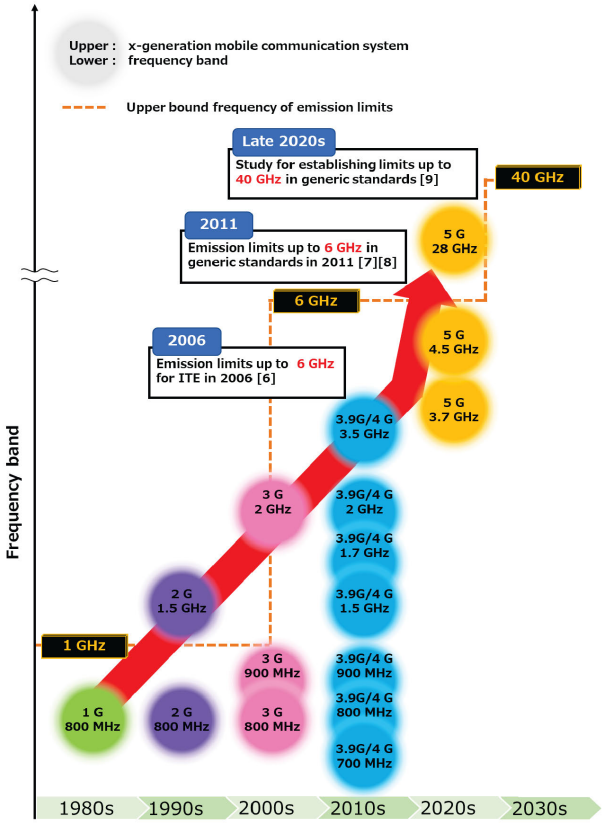

FIGURE 1. Evolution of frequency allocation for mobile communication systems in Japan [1], [2], [3], [4], [5], [6], [7], [8], [9].

The Comité International Spécial des Perturbations Radioélectriques (CISPR) standard is an international standard that provides detailed specifications such as frequencies, measurement methods, facilities, detectors, and limits to protect wireless communication systems from EM disturbances [13], [14]. Generally, radiated emission testing is performed in a fully anechoic room (FAR), which eliminates the effects of external disturbances and wall reflections [9], [15]. CISPR 32 is a standard for radiated emission testing of multimedia equipment [14]. This standard gives specifications for radiated emission testing below 6 GHz in the FAR. Future extension of radiated emission testing up to 40 GHz is being considered to support 5G millimeter-wave devices (see Fig. 1) [9]. However, the reproducibility of test results has become a problem owing to increased insertion losses in the measurement system and the complexity of the radiation directivity of the equipment under test (EUT) with increasing frequency [16]. In contrast, a reverberation chamber (RC) has attracted attention in recent years as an alternative to the FAR, because of its compactness and high sensitivity [17]. The RC, as a cavity resonator that generates a spatially random EM field to emulate a rich isotropic multipath environment with Rayleigh fading in a shielded enclosure, is used in many applications, such as radiated immunity and emission testing [18], shielding effectiveness evaluation [19], antenna efficiency measurement [20], and EM field exposure assessment [21]. In recent years, the RC has also been used for the over-the-air (OTA) evaluation of wireless devices [22]. The EM field in the RC changes randomly owing to the change in boundary conditions by, for example, the rotation of the stirrer. Many of the RC applications mentioned above are performed using the statistics of the EM field or the statistics of the power received by the receiving antenna placed in the RC [18], [19], [20], [21], [22], [23]. Unlike other applications, radiated emission testing does not have a predefined waveform of the EM waves radiated in the RC. In general, the effect of the RC on the received power and the disturbance waveform is unknown owing to the effects of random multipaths in the RC. This can cause problems in correlating the results of radiated emission testing in the FAR with those of testing in the RC.

The first problem is the necessity of the assumption regarding the radiation directivity of the EM disturbance from the EUT. The radiated emission testing in the RC measures the total power of the EM disturbance. On the other hand, current standards are specified in terms of the electric field of the disturbance in the direction of maximum radiation [8]. To convert from total power to an electric field, the directivity of the EUT must be assumed. The other problem is that the disturbance waveform received by a receiving antenna placed in an RC differs from the waveform radiated from the EUT because of the multipaths in the RC. This will cause problems in correlating the test results in the RC with those in the FAR because the difference in the received waveform will cause the measuring receiver to read a different signal strength, even if the detector and resolution bandwidth (RBW) in the measurement are the same as those in the FAR test.

For radiated emission testing, several types of detector are specified in the CISPR 16-1-1 standard, which provides detailed specifications of detector responses to protect wireless systems from continuous or impulsive EM disturbances [13]. This is because the detector response is defined to have a correlation with the effect of the disturbance waveform on the degradation of the reception quality of the interfered wireless receiver. For the FAR radiated emission testing, the limits for peak and average detectors with a bandwidth of 1 MHz (impulse bandwidth) are specified for a measuring receiver above 1 GHz. The purpose of using these detectors is to avoid underestimating both the broadband impulsive and narrowband continuous disturbances. The same detectors as above are also specified for radiated emission testing in the RC [24]. The detector response characteristics specified in the basic standard [13] are divided into two categories: sine wave response and pulse response. The effect of the RC on the detector's response to sine waves can, in principle, be eliminated by performing the calibration by inputting a continuous wave (CW) into the RC and by measuring the RC's output with the specified detector. However, because the disturbance waveforms received in the FAR and RC are generally different for a wideband disturbance waveform, the peak or average detection value of the disturbance also

differs between the FAR and RC [25] even if the received disturbance power is the same as mentioned above, which causes problems in applying the disturbance limits of peak and average detection values in the RC. This difference in detection values depends on the disturbance waveform from the EUT, the characteristics of the RC, the specifications of the detector, and the RBW of the measuring receiver.

In radiated emission testing, the disturbance waveform under test is unknown, and the receiver's RBW must be set in accordance with the applicable standard. To perform radiated emission testing in the RC as an alternative to radiated emission testing in the FAR, it is important to find the conditions under which the detection value relative to the radiated disturbance power is unaffected by the deformation (or distortion) of the disturbance waveform caused by the multipath effects in the RC. In addition, the detection response characteristics with the RC for pulse responses must satisfy the basic standard [13]. To the authors' best knowledge, no previous studies have addressed this problem. In this work, we examine this problem and investigate it experimentally. To investigate the effect of the RC on the detection results, a repetitive pulse train was used to simulate an impulsive disturbance waveform. In Section II, we describe radiated emission testing using the FAR and the RC and the basic configuration of the detector. In Section III, we discuss the challenges of radiated emission testing when using the RC. In Section IV, we evaluate the detection values of the pulse signal using peak, average, and root mean square (RMS) detectors. In Section V, we describe the effect of absorber loading to reduce the time constant of the RC (τ_{RC}) on each detection result.

II. RADIATED EMISSION TESTING ABOVE 1 GHZ

To protect radio services, electronic devices must undergo EMC testing, such as radiated emission testing, and comply with national and regional standards. In this section, we describe radiated emission testing above 1 GHz using the FAR and RC. In addition, the basic configuration of a receiver for measuring EM disturbance is also described.

A. REQUIREMENTS FOR RADIATED EMISSION TESTING ABOVE 1 GHZ

CISPR 32 is a standard for radiated emission testing of multimedia equipment [14]. The requirements for radiated emission testing at frequencies above 1 GHz in a residential environment are shown in Table 1. The radiated emission testing is conducted in the FAR or RC with the average or peak detector. In general, when the FAR is used, the electric field of the EM disturbance is measured, whereas when the RC is used, the total radiated power of the EM disturbance is measured. The limits are specified in terms of the maximum electric field at a specified distance from the EUT, because they are based on an FAR-based model that considers the worst-case probability of occurrence of the maximum directivity of the disturbance from the source pointing at the victim receiver. Therefore, to test the EM disturbance from the EUT in the RC, it is necessary to convert the total radiated power to the maximum disturbance field strength at a specified distance (see Table 1).

TABLE 1. Requirements for radiated emission testing above 1GHz in residential environment [14].

		FAR	RC
Frequency		1 GHz ~ 6 GHz	
Distance		3 m	-
Detector		Average	
		Peak	
Bandwidth		1 MHz	
Limit	(Average)	54 dBμV/m	
	(Peak)	74 dBμV/m	

B. RADIATED EMISSION TESTING IN FAR

Fig. 2 shows a schematic of radiated emission testing above 1 GHz in an FAR. Radiated emission testing above 1 GHz is performed in the FAR with absorbers on the floor [14]. The EUT is placed on a nonconductive table, and the EM disturbance from the EUT is measured by a receiving antenna at a horizontal distance of $R = 3$ m from the EUT. First, the peak radiated directivity of the EUT is determined, and then the EM disturbance is measured by peak detection and average detection and compared with the limit values.

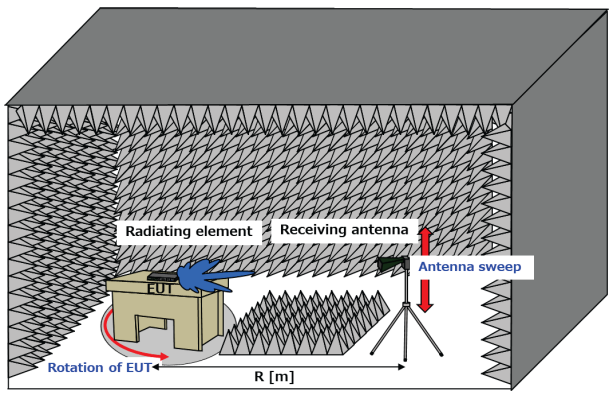

FIGURE 2. Schematic of radiated emission testing in FAR.

C. RADIATED EMISSION TESTING IN RC

Radiated emission testing in an RC is a type of substitution method, which is a method of obtaining the amount of power radiated from the EUT by substitution from the test result of a certain reference quantity [14]. Fig. 3 shows a schematic of radiated emission testing in the RC. The total radiated power from the EUT can be determined from either the average or the maximum received power at the receiving antenna [18], [26]. Before performing radiated emission testing, the RC

must be calibrated. In the RC calibration, the transmitting antenna is placed in the test area and a CW signal is used as the transmit signal. Then, the calibration factors CVF and CLF are defined as follows:

$$\mathrm{CVF} = \left\langle \frac{P_{\mathrm{AveRec}}}{P_{\mathrm{input}}} \right\rangle, \tag{1}$$

$$\mathrm{CLF} = \frac{\mathrm{CVF}}{\mathrm{AVF}}, \tag{2}$$

$$\mathrm{IL} = \left\langle \frac{P_{\mathrm{MaxRec}}}{P_{\mathrm{input}}} \right\rangle, \tag{3}$$

where CVF is the chamber validation factor and is the ensemble average between the transmitting and receiving antennas when the EUT is powered off, P_{AveRec} is the average received power, P_{input} is the average input power into the RC, and $\langle\cdot\rangle$ represents the ensemble average. In addition, CLF is the chamber loading factor and is a combination of the measured results of the EUT calibration and the empty RC calibration, and AVF is the ratio of the average received power to the input power for the empty chamber. Furthermore, IL is the insertion loss obtained from the empty chamber calibration, and P_{MaxRec} is the maximum received power. Finally, the total radiated power from the EUT, as shown in Fig. 3, is defined below as the average or maximum received power at the receiving antenna:

$$P_{\mathrm{rad}} = \frac{\eta_{\mathrm{Tx}} P_{\mathrm{AveRec}}}{\mathrm{CVF}}, \tag{4}$$

$$P_{\mathrm{rad}} = \frac{\eta_{\mathrm{Tx}} P_{\mathrm{MaxRec}}}{\mathrm{CLF} \times \mathrm{IL}}, \tag{5}$$

where η_{Tx} is the efficiency of the transmitting antenna. When testing radiated emissions in the RC above 1 GHz, measurements are performed by peak or average detection for each position of the stirrer. The mean square of the detection values, $\langle P_d^s \rangle$, for a certain detection mode is obtained by sampling and averaging the squared detection value from each angular position.

$$\langle P_d^s \rangle = \frac{1}{N} \sum_{i=1}^{N} \frac{\left(V_{d,i}^s\right)^2}{Z_0} \langle P_d^s \rangle \text{ in W} \tag{6}$$

Here, $V_{d,i}^s$ is the amplitude of the received signal, s is the input signal (pulse or CW), d represents the detector type, N is the number of stirrer steps, and Z_0 is the receiver impedance. If the input signal is the CW, $V_{d,i}^{\mathrm{CW}}$ will be the same for different detectors. However, for signals other than the CW, $V_{d,i}^s$ varies depending on the detector, as shown in the following section, and it should be noted that this difference is also dependent on the waveform input into the receiver. In addition, the mean detection value in terms of amplitude, $\langle V_d^s \rangle$, is defined for the calculation of the maximum field strength $E_{d\_\max}^s$ that is to be compared with the disturbance limits in the FAR [24]:

$$E_{d\_\max}^s = \sqrt{\frac{D_{\max}\eta_0}{4\pi R^2}} \langle V_d^s \rangle, \quad \langle V_d^s \rangle \equiv \sqrt{\langle P_d^s \rangle}, \tag{7}$$

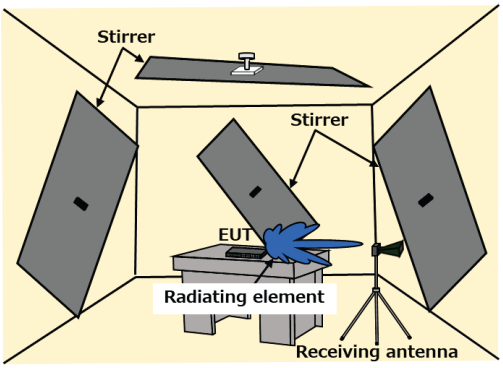

FIGURE 3. Schematic of radiated emission testing in RC.

where $D_{\max}$ is the assumed value of the maximum directivity of the EUT, η_0 is the free space wave impedance, and R is the measurement distance at which the FAR limit value is defined.

D. BASIC CONFIGURATION OF RECEIVER

Fig. 4 shows the basic configuration of a measuring receiver [27]. This configuration is similar to that of a spectrum analyzer, but its frequency selectivity and detection characteristics (CW response and pulse response) are more strictly defined than those of the spectrum analyzer [28]. The specifications of each detector are detailed in CISPR 16-1-1 [13]. As shown in Fig. 4, the envelope of the input tone burst is band-limited by a bandpass filter, followed by envelope detection. In peak detection, the peak envelope amplitude of the band-limited harmonic $e_{\mathrm{RBW}}(t, f_c)$ is displayed as a function of the center frequency f_c of the bandpass filter. For average detection, the envelope amplitude is displayed as being equal to the average value of the filtered disturbance $e_{\mathrm{RBW}}(t, f_c)$. For RMS detection, the envelope amplitude is displayed as being equal to the RMS value of the filtered harmonic $e_{\mathrm{RBW}}(t, f_c)$. Currently, radiated emission testing above 1 GHz has specifications for the peak and the average detectors, but no specifications for the RMS detector. In the case of RMS detection, the right-hand side of (6) corresponds to the power of the EM disturbance, so $\langle P_d^s \rangle$ in (6) represents the total radiated power of the EM disturbance. However, as explained in the next section, when using detectors other than RMS (such as peak and average detectors), it is important to note that $\langle P_d^s \rangle$ calculated using (6) will yield a different value from the total radiated power of the EM disturbance unless the EM disturbance is a CW.

III. CHALLENGE IN RADIATED EMISSION TESTING WITH RC

There are two challenges in radiated emission testing using the RC. One is the necessity of the assumption regarding the radiation directivity of the EM disturbance from the EUT. The other is the effects of the detector and RBW used for radiated

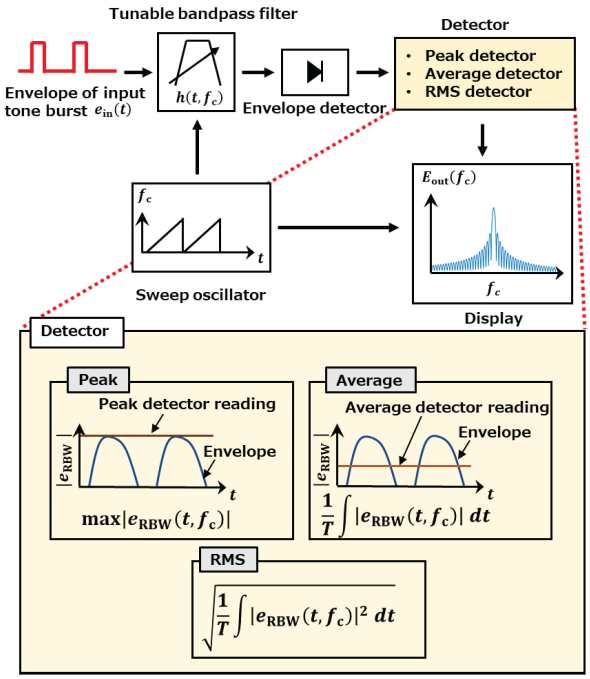

FIGURE 4. Schematic of basic configuration of a receiver for measuring EM disturbance [27].

emission testing on the test results that are compared with the applicable limits.

A. RADIATION DIRECTIVITY OF EUT

The disturbance limits of standards such as CISPR 32 [14] are defined in terms of field strength at a specified distance. For radiated emission testing in the FAR, the peak of the EM disturbance is determined by scanning the azimuth angle, antenna height, and frequency of the EUT in order to find the maximum radiation of the disturbance. The electric field strength of the disturbance is then measured. On the other hand, the radiated emission testing in the RC is used to evaluate the total radiated power in all directions from the EUT. Therefore, to correlate the test results in the RC with those in the FAR, the waveform of the EM disturbance from the EUT at a certain frequency band needs to be independent of the direction. As the frequency increases, it is difficult to determine the direction of maximum disturbance because of the complexity of the directivity pattern of the disturbance radiated from the EUT [16]. Moreover, it is difficult to correlate the test results in the RC with those in the FAR using (7) when two or more EM disturbances with different waveforms are radiated in different directions, as shown in Fig. 5.

B. EFFECT OF RECEIVER DETECTOR AND RBW ON DETECTION VALUE

The FAR is a multipath-free test environment, whereas the RC is a multipath-rich test environment. The EM disturbance from the same EUT is subject to waveform deformation (distortion) due to the presence of multipaths in the RC.

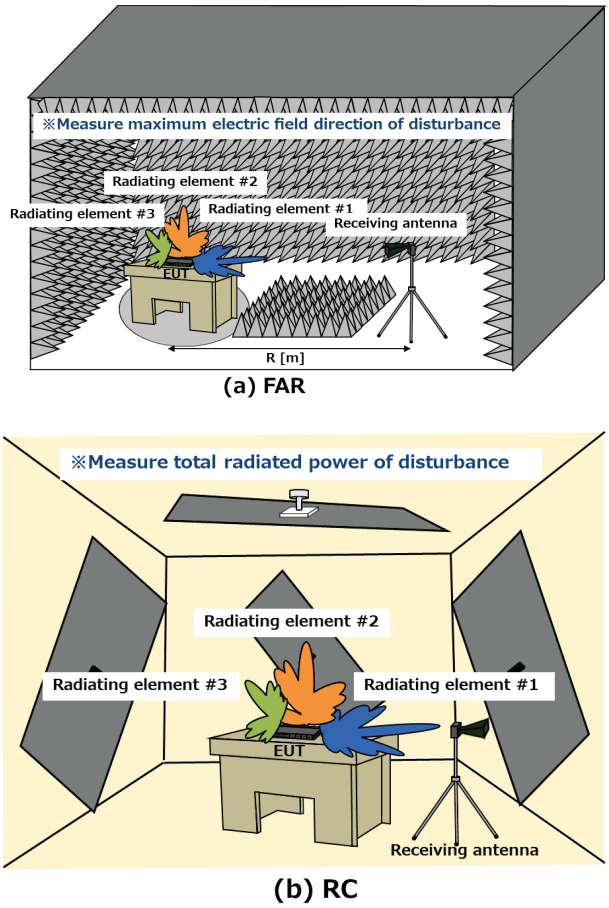

FIGURE 5. Testing of radiated emissions when multiple EM disturbances are present in EUT, for example, impulsive noise from radiating element #1 (cable), continuous noise from radiating element #2 (ventilation slit), and burst noise from radiating element #3 (monitor display), etc.

Owing to this waveform deformation (distortion) in the RC, the detection value of the receiver for the measurement is different from the detection value in the case of no multipath (FAR). This problem may occur when correlating the results of radiated emission testing in the FAR with those in the RC. Fig. 6 shows a schematic of the detector response in EM disturbance measurements using the RC. As an example, pulse signals with pulse widths of 0.1 and 10 μs were input into the RC, and a comparison was made regarding the changes in the pulse waveform (see $|e_i(t, \theta_i)|^2$in Fig. 6) after passing through the RC with various stirrer angles, as shown in Figs. 7(a) and 7(b). Furthermore, a comparison was made regarding the changes in the average envelope waveform of 360 samples for pulse widths of 0.1, 0.5, 1, 5, and 10 μs. Fig. 7(c) shows the results of averaging the time-varying instantaneous power of the output waveform from the RC before passing through the RBW filter, over the stirrer angle. The red line in Fig. 7 represents the envelope of the input pulse waveform, while the lines of different colors represent the envelope waveforms after passing through the RC.

Fig. 7(a) shows the envelope waveforms after passing through the RC at each reference stirrer angle when the input

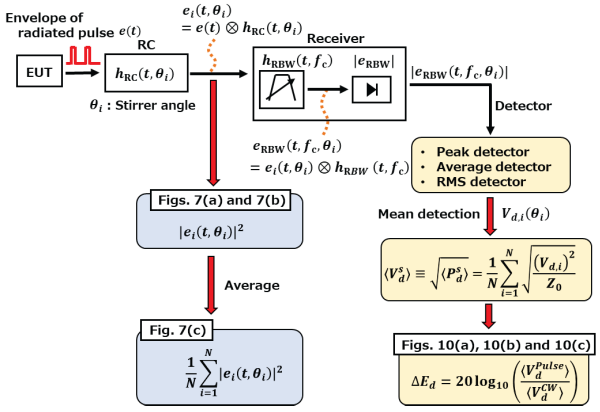

FIGURE 6. Schematic of detector response in EM disturbance measurements using RC.

pulse width is 0.1 μs. The envelope waveform of the received pulse at each stirrer position in the RC is found to be significantly different from that of the input pulse. Fig. 7(b) shows the envelope waveforms after passing through the RC at each reference stirrer angle with a pulse width of 10 μs. When the pulse width is 10 μs, the envelope of the received pulse at each stirrer position in the RC exhibits a gradual decline of the received power, in contrast to the steep fall of the input pulse. Fig. 7(c) shows the average envelope waveforms of 360 samples as the pulse width is varied. For longer pulse widths (10 μs), the received pulse waveform decays after a steady state in which the rising amplitude of the pulse becomes a constant value. For shorter pulse widths (0.1 μs), the waveform decays before the pulse rises sufficiently. The effect of the pulse waveform deformation (distortion) of the averaged envelope also depends on τ_{RC}. The smaller the time constant, the closer the averaged pulse waveform is to the input waveform. As shown by Fig. 7(b), when the radiated pulse width is longer than τ_{RC}, a nearly constant amplitude interval appears in the envelope waveform received within the RC. This is because the RC response reaches a quasi-steady state between pulse widths, and thus, the amplitude within this interval is approximately equal to the received amplitude within the RC when a CW signal with the same amplitude as the input pulse is applied. In other words, it can be corrected by calibrating the RC using CW input. Similarly, when the receiver's RBW is sufficiently narrower than $1/\tau_{RC}$, it is equivalent to using a pulse with a duration of approximately 1/RBW and can be calibrated in a similar manner. On the other hand, as shown in Fig. 7(a), when the pulse width is shorter than τ_{RC}, the received envelope waveform exhibits a random shape. When using a detection mode of the measuring receiver other than RMS, it is not possible to correct the total radiated power expressed in (6) using the calibration results of the RC with the CW.

Fig. 8 shows the relationship between τ_{RC} and the RBW. Fig. 8(a) schematically shows an example when the inverse

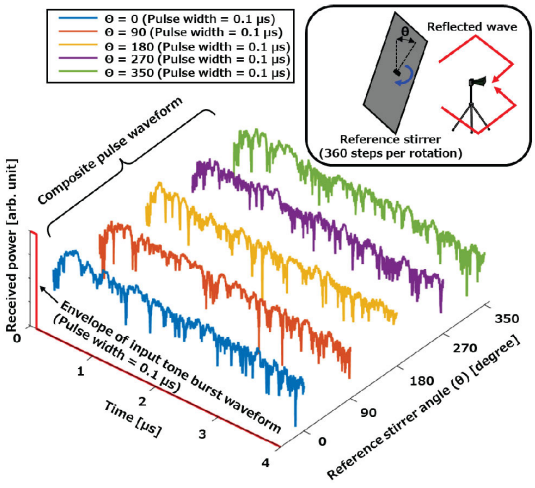

(a) Pulse width = 0.1 μs

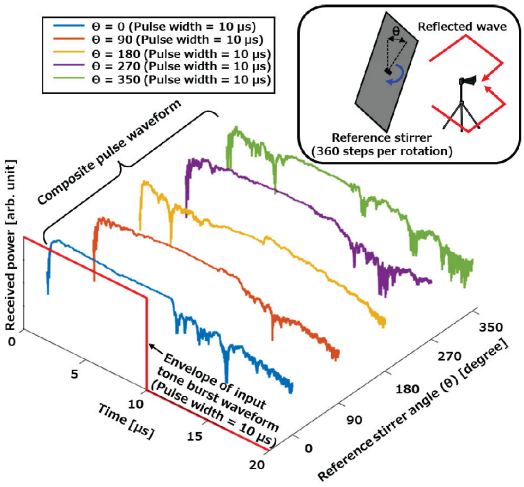

(b) Pulse width = 10 μs

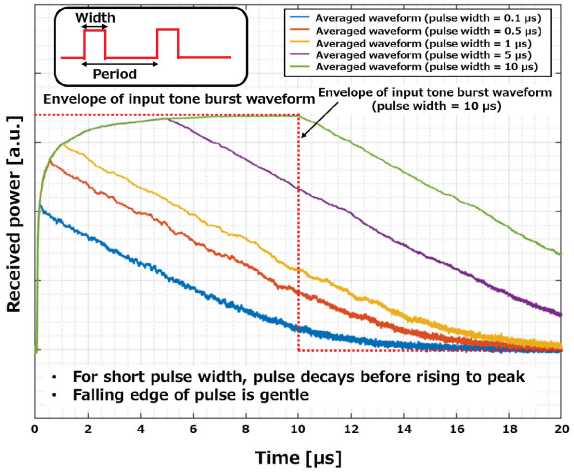

(c) Averaged pulse waveforms of 360 samples

FIGURE 7. Composite pulse waveform of the multipath signal measured in RC. (a) Composite pulse waveform with pulse width of 0.1 μs at stirrer angles (θ) of 0, 90, 180, 270, and 350°. (b) Composite pulse waveform with pulse width of 10 μs at stirrer angles (θ) of 0, 90, 180, 270, and 350°. (c) Averaged pulse waveforms of 360 samples as pulse width varied in RC.

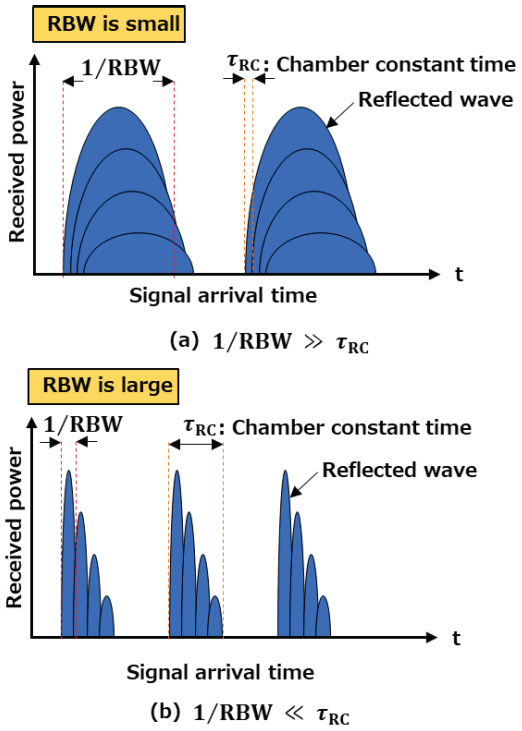

FIGURE 8. Relationship between chamber time constant and RBW.

of the receiver's RBW is greater than τ_{RC}. When the inverse of the RBW is greater than τ_{RC}, all the delayed waves of the signal can be captured during the time of 1/RBW. In this case, the amplitude change due to the overlap of the delayed wave is nearly equal to that of the CW input and can therefore be eliminated by calibrating the RC with CW. This is also pointed out in [18]. When measuring pulse waves in the RC, τ_{RC} should not be greater than 2.5 of the pulse width of the test waveform. Fig. 8(b) illustrates the situation that 1/RBW of the receiver (i.e., the time constant of the receiver filter) is smaller than τ_{RC}. The arrival time of the delayed wave in the RC depends on τ_{RC}; if the inverse of the RBW is smaller than τ_{RC}, it is not possible to capture all of the delayed waves during the time of 1/RBW. Therefore, the envelope amplitude of the received pulses after the band limitation by RBW generally has a random fluctuation, and resultant detection values differ from those of CW depending on the disturbance waveform, the characteristics of the RC, and the detector and RBW of the measuring receiver. In the following sections, we focus on this problem and examine and investigate it experimentally.

IV. MEASUREMENT OF DETECTION VALUE OF PULSE SIGNAL USING VARIOUS DETECTORS IN RC

A. MEASUREMENT SETUP

In this section, the measurement system for evaluating the effect of RC characteristics on the readings of a receiver equipped with a detector and RBW specified in the relevant standard is described. Fig. 9 shows the system for

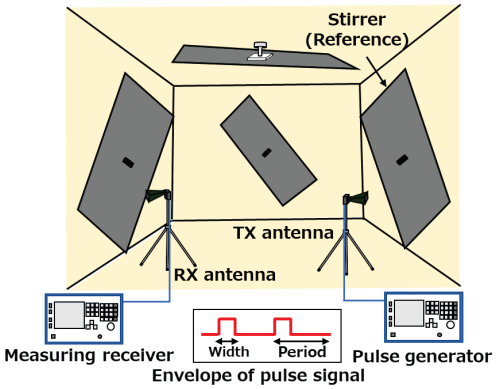

FIGURE 9. Pulse signal measurement in RC.

measuring the detection value of a pulse signal in the RC. The dimensions of the RC are 4 m × 4.5 m × 3 m. This RC is equipped with four stirrers. The reference stirrer rotates at 360 steps per rotation with an angular step of 1°. The other stirrers have different angular steps and rotate at integer multiples of the reference stirrer. A double-ridged horn antenna was used as the transmitting (TX) antenna to simulate the emission from the EUT, and a standard-gain horn antenna was used as the receiving (RX) antenna. The antennas are placed at a height of 1 m above the floor. Both antennas are pointed at different corners to suppress the direct radiation wave to the RX antenna. The antennas are also placed at least 1 m away from the wall to minimize the effect of boundary conditions on the measurement field. The transmitted signal with a pulse train having a carrier frequency of 3.65 GHz is generated by a pulse generator. This frequency is the center frequency of a specific 5G band used in Japan. The study was conducted in the sub-6 band; the methodology in this study is also valid for higher frequencies (e.g., frequency range 2 (FR2) for 5G). The pulse period is set to 100 μs, which is slightly longer than the noise period of the typical switching frequency of the power supply. The pulse width is set to 10, 5, 1, 0.5, and 0.1 μs. The Tx antenna is pointed at the stirrer. The received pulse signal is sent through the RX antenna to a measuring receiver to obtain detection values as a sample is stirred at each angular position. The measurements were performed with peak, average, and RMS detectors (non-CISPR-specified detectors). In this study, measurements were performed in the unloaded state (see Fig. 9) to investigate the effect of τ_{RC} on the mean detection value of the pulses measured by each detector and RBW. Comparative measurements were also performed with τ_{RC} shortened by loading absorbers (1, 2, 4, and 8 absorbers) in the RC. These evaluation results are compared with the results of the simulated FAR test. To eliminate the effect of the measurement environment within FAR on the waveform of the input pulse signal (i.e., residual multipath component in FAR), the measurements were conducted in this simulated FAR test environment in which the pulse generator was directly connected to the receiver, replicating the conditions of the FAR test.

B. EFFECT OF RC ON DETECTION VALUE OF EMISSION MEASUREMENTS IN SUB-6 BAND

Radiated disturbance measurement above 1 GHz is conducted in an FAR that emulates a multipath-free propagation environment, as specified by CISPR basic standards. The FAR provides a multipath-free test environment, while the RC represents a multipath-rich test environment. Therefore, the disturbance detection values obtained through measurements may differ between the FAR and RC. Since the pulse width is generally unknown in radiated disturbance measurements, calibration using CWs or pulses with known time widths cannot eliminate the aforementioned differences. Furthermore, the radiated disturbance measurements specify the RBW and detector characteristics on the basis of the frequency band. Therefore, to discuss the correlation between the FAR and RC, it is necessary to find conditions where τ_{RC} does not affect the measurement RBW or detector characteristics. As discussed in this section, a comparative study was conducted between a simulated FAR test environment, which represents a multipath-free environment, and the RC, which represents a multipath-rich environment, to investigate the differences in the detected values obtained in the two. Fig. 10 shows the difference in the mean detection values of pulse signals between the RC and the simulated FAR calculated by (7) using the peak detector, the average detector (CISPR-specified detectors [13]), and the RMS detector (non-CISPR-specified detectors). The mean detection value ($\langle V_d^s \rangle$) is the result of inputting the disturbance waveforms at each stirrer angle, as shown in Figs. 7(a) and 7(b), into the measuring receiver, detecting the response using the specified detector with bandwidth restriction by RBW, and averaging the results with respect to the stirrer angles. The RBW of the receiver is set to 10, 5, 1, 0.5, and 0.1 MHz, and the mean detection value ($\langle V_d^{\text{Pulse}} \rangle$) of the pulse signal by the RC is normalized by the mean detection value ($\langle V_d^{\text{CW}} \rangle$) of a CW with an input amplitude equal to the peak amplitude of the pulse signal in the FAR. As shown in Fig. 6, the normalized mean detection value (ΔE_d) is defined as

$$\Delta E_d = 20 \log_{10} \left(\frac{\langle V_d^{\text{Pulse}} \rangle}{\langle V_d^{\text{CW}} \rangle} \right) \Delta E_d \text{ in dB}. \tag{8}$$

When $\langle V_d^{\text{Pulse}} \rangle$ and $\langle V_d^{\text{CW}} \rangle$ are equal, this normalized mean detection value (ΔE_d^s) will be zero, and equivalent results are obtained for both RC and FAR tests. In addition, peak value desensitization occurs in the FAR as the product of RBW and pulse width decreases. The RBW of the receiver above 1 GHz is specified as the impulse bandwidth (B_{imp}), and the peak detection value of the filter output when a narrow pulse is input is proportional to the product of B_{imp} and the input pulse width. The same trend is also observed for the RC. The difference with the simulated FAR increases particularly when the RBW is wide and the pulses are short. This is because the coherent bandwidth of the RC has become narrower than the RBW (in other words, the delay spread or time constant has become larger than 1/RBW), and in effect, the impulse bandwidth of the measurement system using the RC has become narrower than the RBW of the receiver.

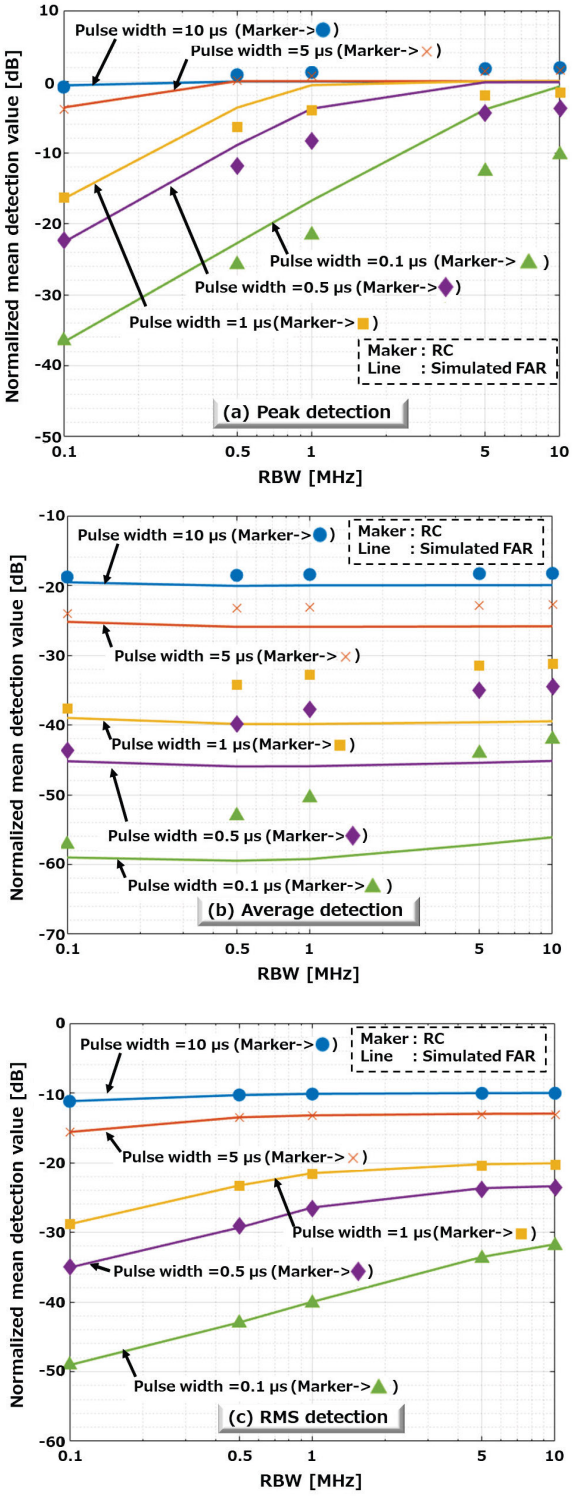

FIGURE 10. Difference between mean detection values of repetitive pulses in RC and simulated FAR (pulse period = 100 μs).

Fig. 10(a) shows the results (ΔE_{Peak}) of peak detection. The difference between the test results obtained in the RC and

the simulated FAR became larger as the pulse width became smaller, as described above. The peak amplitude of the signal waveform received in the RC at a certain stirrer angle is a random variable, and the normalized mean detection value calculated by (7) for all stirrer angles depends on τ_{RC}, which indicates the charging time until the signal amplitude reaches a steady state due to multiple reflections in the RC [29]. When the pulse width is longer than 5 μs, the normalized mean detection value in the RC is almost the same as that in the simulated FAR.

Otherwise, the mean detection value in the RC is smaller than that in the simulated FAR. This is because the received pulse signal waveform in the RC decays (in the statistical sense) before reaching a steady state, as shown in Fig. 7(c). We also observed that the mean detection value of the peak detector is slightly larger than the simulated FAR results for pulse widths of 5 and 10 μs, because the frequency response is not flat within the RBW of the receiver in the RC. As the RBW increases, the multiple-reflection effect becomes more significant. When the RBW is multiplied by the pulse width, desensitization occurs as the RBW becomes smaller [30].

Fig. 10(b) shows the results ($\Delta E_{\text{Average}}$) of the average detection. As the pulse width became smaller, the difference between the test results in the RC and those in the simulated FAR became larger. This is due to the different pulse waveform changes in the RC. As shown in Figs. 7(a) and 7(b), the input waveform to the RC and the received waveform are completely different. In particular, the pulse waveform was observed to fall gradually rather than steeply. This depends on τ_{RC} and can be improved by installing absorbers. In addition, the effect of the mean detection value is especially conspicuous when the RBW of the receiver increases. Furthermore, the mean detection value with the pulse width of 10 μs is about -20 dB, which is approximately equal to the ratio of the pulse width to the period.

Fig. 10(c) shows the results (ΔE_{RMS}) of RMS detection. We confirmed that the relative changes in the mean detection values in the RC and the simulated FAR with respect to the changes in the pulse width and RBW are in good agreement. In RMS detection, the effect of pulse desensitization in the RC and simulated FAR on the mean detection value is found to be almost the same. Furthermore, when the RBW multiplied by the pulse width of the input signal is greater than 2.5, the mean detection value for both the RC and the simulated FAR decreases in proportion to the pulse width. Besides, the mean detection value with a pulse width of 10 μs is about -10 dB, which is approximately equal to the square of the ratio of the pulse width to the period.

C. EFFECT OF RC ON DETECTION VALUE OF EMISSION MEASUREMENTS IN FR2 BAND

As discussed in this section, the effect of RC characteristics on the readings of a receiver equipped with a detector and RBW is investigated in the FR2 band where the measurement system and propagation losses are much greater than those in the Sub-6 band. To maintain signal quality, a small RC was used in the study. Fig. 11 shows the system for measuring the detection value of a pulse signal in the small RC. The dimensions of the RC are 1.2 m $\times$ 0.8 m $\times$ 1 m. This RC is equipped with two stirrers. The reference stirrer rotates at 360 steps per rotation with an angular step of 1°. The other stirrer has different angular steps and rotates at integer multiples of the reference stirrer. Ridged horn antennas were used as the TX and RX antennas. Both antennas are pointed at different corners to suppress the direct radiation wave to the RX antenna. The transmitted signal with a pulse train having a carrier frequency of 27.5 GHz is generated by a pulse generator. The pulse period and pulse width were set to the same parameters as described in Section IV-A.

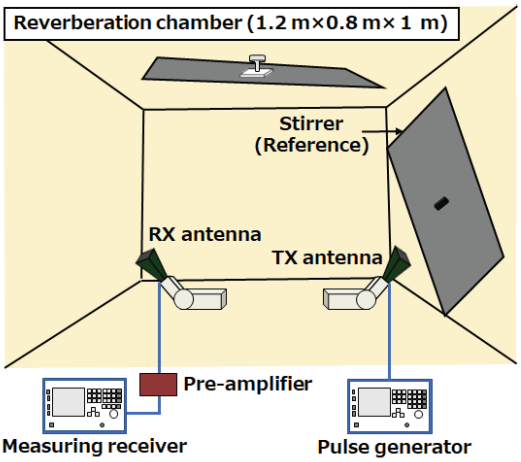

FIGURE 11. Pulse signal measurement in small RC.

Fig. 12 shows the difference in the mean detection values of pulse signals between the small RC and the simulated FAR calculated with (8) using the peak detector, the average detector, and the RMS detector. Fig. 12(a) shows the results (ΔE_{Peak}) of peak detection. Unlike the case of Sub-6 band measurement using the large RC, we confirmed that the relative changes in the mean detection values in the small RC and the simulated FAR with respect to the changes in the pulse width and RBW are in good agreement, except for the pulse width of 0.1 μs. The reason is that the chamber time constant ($\tau_{RC} = 206.0$ ns) of the small RC is smaller than the chamber time constant ($\tau_{RC} = 2132.7$ ns) of the large RC. When τ_{RC} multiplied by the RBW is less than 0.35, the difference between the mean detection values of the peak detector in the FAR and RC becomes less than 1 dB. Fig. 12(b) shows the results ($\Delta E_{\text{Average}}$) of the average detection. As the pulse width became smaller, the difference between the test results in the RC and the simulated FAR became larger. This is due to the different pulse waveform changes in the RC, as in the case of the large RC. Fig. 12(c) shows the results (ΔE_{RMS}) of RMS detection. As in the case of the large RC, we confirmed that the relative changes in the mean detection values in the RC and with the simulated FAR with respect to the changes in the pulse width and RBW are in good agreement.

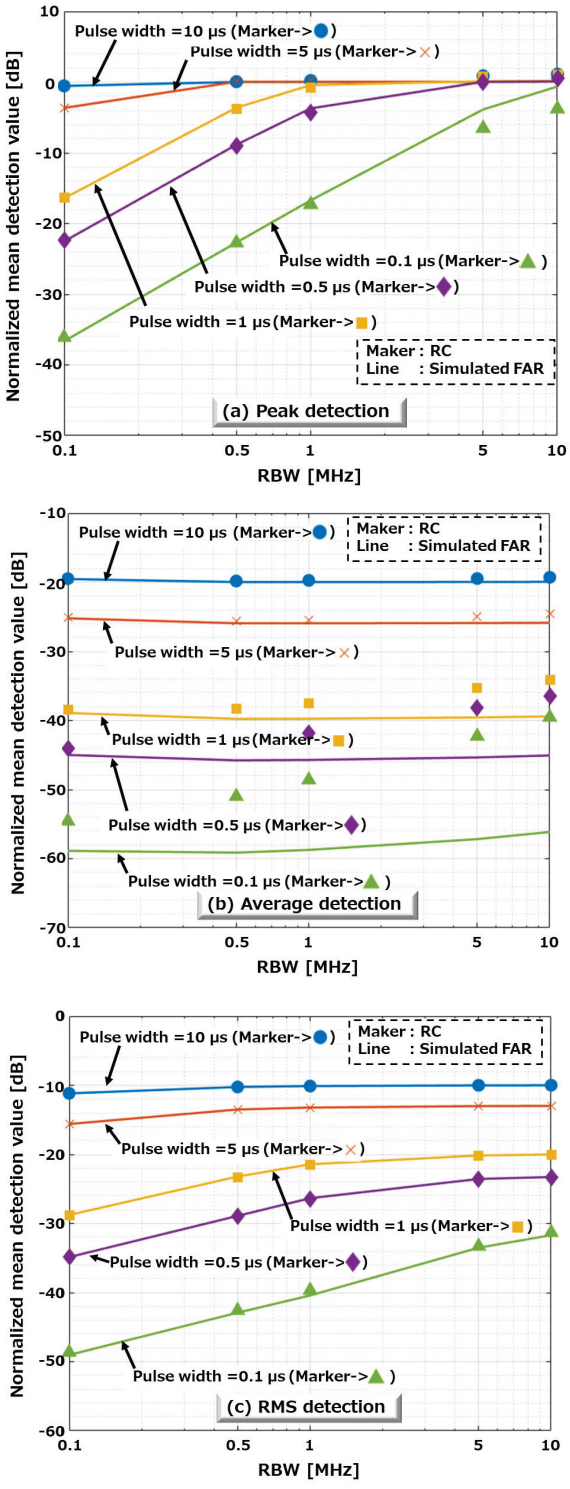

FIGURE 12. Difference between mean detection values of repetitive pulses in small RC and simulated FAR (pulse period = 100 μs).

V. IMPROVEMENT OF MEAN DETECTION VALUE WITH ABSORBERS

The difference between the mean detection values of impulsive disturbance measured in the RC and the simulated FAR is caused by the increase in the delay spread (in other words,

TABLE 2. Chamber time constants (τ_{RC}) in RC with various numbers of absorbers (Size: 60 × 60 × 30cm^2).

Number of absorbers	0	1	2	4	8
Chamber time constant [ns]	2132.7	596.1	347.1	193.3	99.3

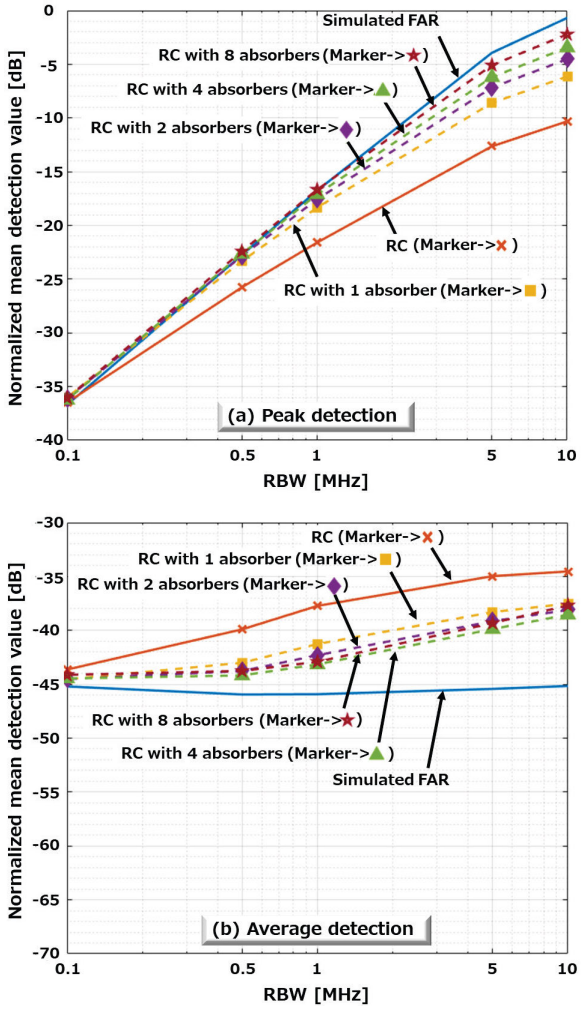

FIGURE 13. Effect of absorber on mean detection value (Pulse bandwidth = 0.1 μs).

the reduction in the coherent bandwidth) of the received disturbance owing to the multiple reflections within the RC. This effect can be reduced by installing absorbers in the RC to reduce τ_{RC} to the extent that the coherent bandwidth becomes sufficiently wider than the RBW specified for radiated emission testing. On the other hand, the loss of the RC will be significantly increased, thus reducing the sensitivity of the measurement.

Numerous studies have focused on the characterization of RC, specifically on the reduction of τ_{RC} through the addition of absorbers [31]. However, there is little discussion regarding the effect of absorbers on radiated emission testing,

particularly in relation to detector response. In this section, the reduction of τ_{RC} upon introducing absorbers and the associated improvement of the detection characteristics are discussed. Table 2 shows the chamber time constants for different numbers of absorbers. The data clearly show that τ_{RC} decreases as the number of absorbers in the RC increases.

Then, the peak and average detection with the absorber in the RC are investigated. Fig. 13 shows the results of the detection characteristics in the RC with and without absorbers. Fig. 13(a) shows the results of peak detection when the pulse bandwidth is 0.1 μs. The normalized mean detection values in the RC approach those with the simulated FAR as the number of absorbers increases. When τ_{RC} multiplied by the RBW is much smaller than 0.35, the difference between the mean detection values in the RC and the simulated FAR is less than 1 dB. Considering the decrease in the sensitivity of the measurement owing to the presence of the absorber, the average detection is examined for signals with a pulse bandwidth of 0.5 μs. Fig. 13(b) shows the effect of the absorber on the mean detection values of the average detection. The mean detection values in the RC with absorbers are slightly closer to the simulated FAR results than those without absorbers. However, when the number of absorbers is increased to 8, the mean detection values are conversely worse.

VI. CONCLUSION

To enable radiated emission testing in the RC as an alternative method to radiated emission testing in the FAR, it is important that the readings of the measuring receiver with a detector specified in the relevant standards are unaffected by the characteristics of the RC. In this study, we investigated the conditions under which the detection values of impulsive disturbances measured in the FAR are equivalent to those in the RC, using the peak detector, the average detector (CISPR-specified detectors), and the RMS detector (non-CISPR-specified detectors) and the RBW of the receiver for radiated emission testing in the FAR. For peak detection, the result in the RC depends on τ_{RC} and the RBW. The shorter the pulse width, the greater the difference between the RC result and the FAR result. When τ_{RC} multiplied by the RBW is less than 0.35, the difference between the mean detection values of the peak detector in the FAR and RC becomes less than 1 dB. For both average and peak detections, the result in the RC depends on the time-constant characteristic of the RC. Compared with the RMS detection, the mean detection value of the average detection is more sensitive to the signal waveform. The installation of absorbers brought the RC results closer to the FAR results, but increasing the number of absorbers may degrade the signal-to-noise ratio (SNR) required for the measurement. The effect of waveform deformation on the detection response can be reduced by inserting absorbers into the RC to shorten the time constant, but this is a trade-off with the measurement sensitivity (lower SNR) in the RC. In the pulse measurement using RMS detection, the relative changes in the mean detection values in the RC agree well with those in the FAR for all pulse widths and RBWs.

REFERENCES

[1] R. Dilli, "Analysis of 5G wireless systems in FR1 and FR2 frequency bands," in *Proc. 2nd Int. Conf. Innov. Mech. Ind. Appl. (ICIMIA)*, Mar. 2020, pp. 767–772.

[2] Telecommunications Bureau and Ministry of Public Management, Home Affairs, Posts and Telecommunications (MPHPT). (Aug. 2001). *Outline of the Telecommunications Business in Japan*. [Online]. Available: https://www.soumu.go.jp/main_sosiki/joho_tsusin/eng/Statistics/yellowbook/YB0108.pdf

[3] KDDI Corporation. (2020). *Integrated Report 2020*. [Online]. Available: https://www.kddi.com/extlib/files/english/corporate/ir/library/annual_report/pdf/kddi_ar2020_e.pdf

[4] Y. Sagae, S. Sawamukai, Y. Ohwatari, K. Kiyoshima, K. Kanbara, and J. Takahashi, "5G network," *NTT Tech. Rev.*, vol. 18, no. 12, pp. 86–96, Dec. 2020.

[5] *Ministry of Internal Affairs and Communications Homepage (in Japanese Only)*. Accessed: Jul. 27, 2023. [Online]. Available: https://www.soumu.go.jp/main_content/000692919.pdf

[6] *Information Technology Equipment—Radio Disturbance Characteristics—Limits and Methods of Measurement*, Standard CISPR 22, 2006.

[7] *Electromagnetic Compatibility (EMC)—Part 6–3: Generic Standards—Emission Standard for Equipment in Residential Environments*, Standard CISPR 16-6-3, 2011.

[8] *Electromagnetic Compatibility (EMC)—Part 6–4: Generic Standards—Emission Standard for Industrial Environments*, Standard CISPR 16-6-4, 2011.

[9] R. Vick, J. Petzold, M. Rosenthal, and J. Kasper, "Investigation of emission requirements above 1 GHz towards 5G," *2020 Int. Symp. Electromagn. Compat. - EMC Eur.*, vol. 2020, pp. 1–8.

[10] *IEEE Standard for Safety Levels With Respect to Human Exposure to Electric, Magnetic, and Electromagnetic Fields, 0 Hz to 300 GHz*, Standard IEEE C95.1-2019, 2020. [Online]. Available: https://standards.ieee.org/standard/C95_1-2019.html

[11] R. Dilli, "Implications of mmWave radiation on human health: State of the art threshold levels," *IEEE Access*, vol. 9, pp. 13009–13021, 2021.

[12] International Commission on Non-Ionizing Radiation Protection, "Principles for non-ionizing radiation protection," *Health Phys.*, vol. 118, no. 5, pp. 477–482, May 2020.

[13] *Specification for Radio Disturbance and Immunity Measuring Apparatus and Methods Part 1–1: Radio Disturbance and Immunity Measuring Apparatus—Measuring Apparatus*, Standard CISPR 16-1-1, 2019.

[14] *Electromagnetic Compatibility of Multimedia Equipment—Emission Requirements*, Standard CIS/I/655/CD CISPR 32, 3rd ed., 2022.

[15] X. Wang and R. Vick, "Determination of radiated emissions of an electrically large EUT: Simulation and experiment," in *Proc. IEEE Int. Symp. Electromagn. Compat. (EMC)*, Aug. 2015, pp. 295–299.

[16] W. Zhang, Z. Peng, X. Wang, D. Kim, and J. Drewniak, "Radiated emission tests for high-frequency router systems in class A: Discussion and improvement," in *Proc. IEEE Int. Joint EMC/SI/PI EMC Eur. Symp.*, Jul. 2021, pp. 119–124.

[17] F. B. J. Leferink, "Using reverberation chambers for EM measurements," in *Proc. 18th Int. Conf. Softw., Telecommun. Comput. Netw. (SoftCOM)*, Sep. 2010, pp. 1–5.

[18] *Electromagnetic Compatibility (EMC)—Part 4–21: Testing and Measurement Techniques—Reverberation Chamber Test Methods*, Standard IEC 61000-4-21, International Electrotechnical Commission, Geneva, Switzerland, 2011.

[19] C. L. Holloway, D. A. Hill, M. Sandroni, J. M. Ladbury, J. Coder, G. Koepke, A. C. Marvin, and Y. He, "Use of reverberation chambers to determine the shielding effectiveness of physically small, electrically large enclosures and cavities," *IEEE Trans. Electromagn. Compat.*, vol. 50, no. 4, pp. 770–782, Nov. 2008.

[20] C. L. Holloway, H. A. Shah, R. J. Pirkl, W. F. Young, D. A. Hill, and J. Ladbury, "Reverberation chamber techniques for determining the radiation and total efficiency of antennas," *IEEE Trans. Antennas Propag.*, vol. 60, no. 4, pp. 1758–1770, Apr. 2012.

[21] D. Senic, A. Sarolic, C. L. Holloway, and J. M. Ladbury, "Whole-body specific absorption rate assessment of lossy objects exposed to a diffuse field inside a reverberant environment," *IEEE Trans. Electromagn. Compat.*, vol. 59, no. 3, pp. 813–822, Jun. 2017.
[22] C. L. Patané, A. Skårbratt, and C. Orlenius, "Basic and advanced MIMO OTA testing of wireless devices using reverberation chamber," in *Proc. 8th Eur. Conf. Antennas Propag. (EuCAP)*, Apr. 2014, pp. 3488–3492.
[23] K. A. Remley, C. J. Wang, D. F. Williams, J. J. A. D. Toorn, and C. L. Holloway, "A significance test for reverberation-chamber measurement uncertainty in total radiated power of wireless devices," *IEEE Trans. Electromagn. Compat.*, vol. 58, no. 1, pp. 207–219, Feb. 2016.
[24] *Amendment 2: Specification for Radio Disturbance and Immunity Measuring Apparatus and Methods—Part 4–5: Uncertainties, Statistics and Limit Modelling—Conditions for the Use of Alternative Test Methods*, Standard CISPR TR 16-4-5, 2020.
[25] L. R. Arnaut and D. A. Knight, "Observation of coherent precursors in pulsed mode-stirred reverberation fields," *Phys. Rev. Lett.*, vol. 98, no. 5, pp. 053903-1–053903-4, Feb. 2007.
[26] H. G. Krauthuser, "On the measurement of total radiated power in uncalibrated reverberation chambers," *IEEE Trans. Electromagn. Compat.*, vol. 49, no. 2, pp. 270–279, May 2007.
[27] Y. Matsumoto, K. Fujii, and A. Sugiura, "Estimating the amplitude reduction of clock harmonics due to frequency modulation," *IEEE Trans. Electromagn. Compat.*, vol. 48, no. 4, pp. 734–741, Nov. 2006.
[28] *Measuring With Modern Spectrum Analyzers, Educational Note*, Rohde-Schwarz, Munich, Germany, 2013.
[29] M. L. Crawford and G. H. Koepke, "Preliminary evaluation of reverberation chamber method for pulsed RF immunity testing," in *Proc. IEEE Int. Symp. Electromagn. Compat.*, Sep. 1986, pp. 1–9.
[30] *Pulsed RF Calculator, Application Note*, Rohde-Schwarz, Munich, Germany, 2015.
[31] C. L. Holloway, H. A. Shah, R. J. Pirkl, K. A. Remley, D. A. Hill, and J. Ladbury, "Early time behavior in reverberation chambers and its effect on the relationships between coherence bandwidth, chamber decay time, RMS delay spread, and the chamber buildup time," *IEEE Trans. Electromagn. Compat.*, vol. 54, no. 4, pp. 714–725, Aug. 2012.

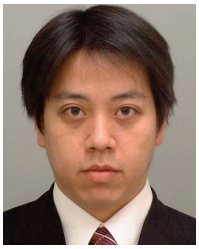

IFONG WU received the B.E., M.E., and D.E. degrees in electrical engineering and electronics from Aoyama Gakuin University, Kanagawa, Japan, in 2000, 2002, and 2007, respectively. In 2007, he joined the National Institute of Information and Communications Technology (NICT), Tokyo, Japan, as a Senior Researcher, where he has been engaged in research on the electromagnetic compatibility of radio communication systems. He is an expert member of IEC SC77B/CISPR/A/JTF TEM.

SADAAKI SHIOTA received the B.E. degree in engineering from Utsunomiya University, Tochigi, Japan, in 1995. In 2012, he joined the National Institute of Information and Communications Technology (NICT), Tokyo, Japan, where he has been engaged in the research and development of type approval test and radio equipment testing methods. He is currently engaged in research on communication EMC. His research interest includes the design and development of marine radar.

YASUSHI MATSUMOTO (Member, IEEE) received the B.E., M.E., and Ph.D. degrees in electrical and communication engineering from Tohoku University, Sendai, Japan, in 1983, 1985, and 1998, respectively. In 1985, he joined the Radio Research Laboratory [currently, National Institute of Information and Communications Technology (NICT)], where he is currently a member of the Electromagnetic Compatibility Laboratory, Radio Research Institute. From 1990 to 1994, he was with the National Space Development Agency, Japan [currently, the Japan Aerospace Exploration Agency (JAXA)]. From 1999 to 2005, he was an Associate Professor with Tohoku University. He has been engaged in the study of satellite communications, EMC in wireless systems, and EMC measurement. He is an expert member of CISPR SC/H. He was a recipient of the 2009 IEICE Communications Society Best Paper Award, the EMC 2009 Kyoto International Symposium Excellent Paper Award, and the 2011 IEEE Richard Schulz Transactions Prize Paper Award.

KAORU GOTOH (Member, IEEE) received the B.E., M.E., and Ph.D. degrees in electrical engineering with signal processing from The University of Electro-Communications, Tokyo, Japan, in 1996, 1998, and 2002, respectively. From April 2001 to March 2002, she was a Visiting Scholar with Saint Petersburg State University, Russia. In 2003, she joined the National Institute of Information and Communications Technology, Tokyo, where she is currently the Research Manager with the Electromagnetic Compatibility Laboratory. Her current research interest includes EMC for wireless communication systems. She was s recipient of the 2011 Richard Schulz Transactions Prize Paper Award from the IEEE EMC Society.